Sheetlike Side-Chain Liquid Crystalline Polyacetylenes Forming Monolayer Lamellae in Dilute Solutions

Zhen-Qiang Yu,[†] Jia-Hao Liu,[†] Jing-Jing Yan,[†] Xuan-Bo Liu,[†] De-Hai Liang,[†] Jacky W. Y. Lam,[‡] Yu-Ping Dong,[§] Zi-Chen Li,[†] Er-Qiang Chen,*[,†] and Ben Zhong Tang*[,‡]

Beijing National Laboratory for Molecular Sciences, Department of Polymer Science and Engineering and the Key Laboratory of Polymer Chemistry and Physics of the Ministry of Education, College of Chemistry and Molecular Engineering, Peking University, Beijing 100871, China; Department of Chemistry, The Hong Kong University of Science & Technology, Clear Water Bay, Kowloon, Hong Kong, China; and College of Material Science and Engineering, Beijing Institute of Technology, Beijing 100871, China

Received May 2, 2007; Revised Manuscript Received August 27, 2007

ABSTRACT: Self-assembly behaviors of a series of hydrophobic side-chain liquid crystalline (LC) polyacetylenes, namely, poly(5-{[(4′-alkoxy-4-biphenylyl)carbonyl]oxy}-1-pentyne)s [P-3,*m* (*m* = 5, 7, 9)], were studied in dilute solutions. The assembly was induced by tuning the solvent property to be selective for the alkyl tails on the side chains, with the processes characterized by turbidity, dynamic light scattering, ^{1}H NMR, and excitation fluorescence anisotropy measurements. The morphology and structure of the P-3,*m* aggregates formed in the solutions were investigated using atomic force microscopy and wide-angle X-ray diffraction. The experimental results indicate that the P-3,*m* polymers can form monolayer lamellae in selective solvents. In the lamella, the P-3,*m* molecules are sheetlike and pack parallel to each other with their backbones located in the lamellar center and their alkyl tails covering the top and bottom lamellar surfaces. The lamellar thickness is largely determined by the width of the molecular sheet. When the solvent becomes selective for the tails, the P-3,*m* chains may undergo shape stiffening to become more sheetlike.

Introduction

At the molecular structure level, side-chain liquid crystalline (LC) polymers always bear chemical heterogeneity.[1−4] Therefore, they may adopt "microphase separation" structure in both thermotropoic and lyotropic LC phases.[5−13] In smectic or lamellar phases, the backbones incompatible with the side chains form a sublayer squeezed by two adjacent side-chain sublayers. Since mesogenic cores always tend to pack parallel to each other, their separation from spacers/tails on side chains can further develop. Similar "microphase separation" has also been found in side-chain LC polymers in columnar or hexagonal phases. For example, the monodendron-jacketed polymers may have the radial phase separation between the backbones and the side chains containing aromatic cores and alkyl tails that results in molecular cylinders.

One may ask whether such a "microphase separation" will lead to self-assembly of side-chain LC polymers in dilute solutions. In this regard, the studies on side-chain polyamphiliphiles have revealed important features.[10,14−18] In aqueous solutions of side-chain polyamphiliphiles, the hydrophobic parts can form microdomains that are surrounded by the shells of the hydrophilic parts, the structures of which are similar to micelles of small molecular surfactants[1,19] or block copolymers[20] in selective solvents. The micelle formation of the side-chain polyamphiliphiles depends largely on the chemical structures and molecular architectures. For example, different accommodation of the hydrophilic head of the surfactant side chains may substantially alter the hydrophilic−hydrophobic balance of the polymers, thus resulting in the formation of different aggregates in aqueous solutions. The flexibility of the polymer backbone is also important. As the local density of the surfactant side chains is rather high, the polymers with highly flexible backbones can form intramolecular aggregates. Therefore, the critical micelle concentration (cmc) may be missing. For the rodlike side-chain polyamphiliphiles, intermolecular aggregation is favored. It has been reported that poly[*p*-(alkyl)phenylsulfonate]s form cylindrical micelles in aqueous solution, with the radial aggregation number determined by the volume and shape of the hydrophobic segments per repeating unit.[18]

In this study, using a series of poly(5-{[(4′-alkoxy-4-biphenylyl)carbonyl]oxy}-1-pentyne) [see Chart 1, abbreviated as P-3,*m* (*m* = 5, 7, 9)] as an example, we report our investigation on the self-assembly of the fully hydrophobic side-chain LC polyacetylene in dilute solutions. In contrast to shape-persistent polymers including side-chain polyacetylenes which are often rodlike or wormlike,[7,8,18,21−25] the molecules we studied are somewhat sheetlike due to the rigid and extended conjugated backbone and the short spacer of three methylene units in the side chains. P-3,7 in bulk state forms a highly ordered smectic phase with a frustrated molecular packing.[26] The building blocks of the LC phase are the whole P-3,7 molecular sheets rather than the mesogens. The same LC structure was also found in P-3,5 and P-3,9. For our dilute solution study, the primary goal was to understand when the solvent property was finely tuned, whether the different chemical ingredients within the polymer chains could render sufficient solvophobicity difference that could lead to ordered nanostructure rather than macroscopic precipitation. We demonstrate that the polymers can self-assemble into monolayer lamellae in solvents that are selective for the alkyl tails, wherein the sheetlike molecules pack parallel

* To whom correspondence should be addressed. E-mail: eqchen@pku.edu.cn (E.Q.C.) and tangbenz@ust.hk (B.Z.T.).
† Peking University.
‡ The Hong Kong University of Science & Technology.
§ Beijing Institute of Technology.

10.1021/ma0710028 CCC: $37.00
Published on Web 10/13/2007

Chart 1. Chemical Structure of the Side-Chain LC Polyacetylenes [P-3,*m* (*m* = 5, 7, and 9)]

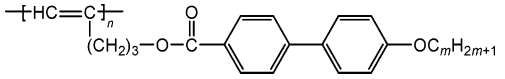

to each other and the lamellar thickness is largely determined by the sheet width. Our experiment suggests that the molecular shape undergoes rigidification to be more sheetlike when the solvent becomes poorer for the mesogenic cores.

Experimental Section

The synthesis of P-3,*m* has been published.[4,27] In brief, using WCl_6-Ph_4Sn as a catalyst tolerant of the functional groups on the substitutes of the acetylene monomers, the solution polymerization under optimal condition yielded the polymers with moderate to high molecular weights (MW) and predominantly trans structure of good stereoregularity. For the samples used in this study, the apparent number-average MWs of around 20×10^3 and polydispersity of 2 were measured by gel permeation chromatography (GPC) using polystyrene standards, and the trans contents of >80% were determined from ^{1}H NMR analysis.

The stock solutions of P-3,*m* in the concentration range of $10^{-4}-10^{-2}$ g/mL were prepared by dissolving the polymers in chloroform (C), which is a common solvent for all components of the side chains, and were stored overnight. Afterward, a selective solvent for the alkyl tails, such as *n*-dodecane (D), *n*-octane (O), or cyclohexane (CH), was gradually dropped into the stock solution to the desired selective/common solvent volume ratios (v/v) and concentrations. To describe the thermal behavior of the solution self-assembly, we here chose P-3,7 in CH/C (v/v = 9/1) as an example because this system with concentration of $10^{-5}-10^{-3}$ g/mL was found to exhibit a transition temperature range from 20 to 55 °C, which was accessible by the experimental techniques used.

Turbidity and UV−vis absorption measurements were carried out using a Cary 1E UV−vis spectrometer. The turbidity was recorded at a wavelength of 750 nm where the absorptions are the lowest for the polymer, solvent, and aggregate solutions, and the solvent was used as the reference. The solution turbidity varying with the selective/common solvent volume ratio was measured at room temperature. After a certain amount of the selective solvent was added, the solution was equilibrated for 20 min before measurement. The turbidity of P-3,7 in CH/C (v/v = 9/1) as a function of temperature was measured upon cooling and heating process. At each set temperature the solution was stayed isothermally for 20 min.

The dynamic light scattering (DLS) cooling experiments of P-3,7 in CH/C (v/v = 9/1) were performed on a Brookhaven goniometer (BI-200SM) equipped with a BI-TurboCorr digital correlator and a thermostatic bath with temperature accuracy of ±0.01 °C. The vertically polarized laser beam was supplied by a solid-state laser source (Mini L-30, Brookhaven, 30 mW) operating at 636 nm. The stock solution was filtered through Millipore 0.22 μm PTFE filter into a dust-free vial and then diluted with filtered cyclohexane to 1×10^{-4} g/mL. During cooling, the autocorrelation functions at 30°, 60°, and 90° were collected in the homodyne mode immediately after the sample was stayed for 10 min at each set temperature. The time correlation functions were analyzed with a Laplace inversion program CONTIN. The viscosity of the mixed solvent at different temperature was measured using Ubbelohde viscometer, and the refractive index was calculated as the volume-weighted average of solvent components.

The temperature-dependent ^{1}H NMR spectra and steady-state fluorescence anisotropies were measured for P-3,7 in CH/C (v/v = 9/1). At each preset temperature, the sample was allowed to equilibrate for 20 min. The ^{1}H NMR spectra of the sample in deuterated solvents were recorded on a Bruker Advance 400 MHz spectrometer using tetramethylsilane as the internal reference. The steady-state fluorescence spectra and excitation fluorescence anisotropies were measured on a Hitachi F4500 fluorescence spectrometer. For comparison, the fluorescence of P-3,7 in pure chloroform were also examined. The excitation and emission spectra were recorded at $\lambda_{em} = 370$ nm and $\lambda_{ex} = 310$ nm, respectively, using slits with band-pass of 5 nm for both monochromators. To determine fluorescence anisotropies, the filter polarizers of the spectrometer were aligned in L-format configuration. The excitation anisotropy value (r) was calculated from $r = (I_{VV} - GI_{VH})/(I_{VV} + 2GI_{VH})$, where I_{VV} and I_{VH} are the fluorescence intensities polarized parallel and perpendicular to the excitation light at $\lambda_{em} = 370$ nm, respectively, and G is the instrumental correction factor of I_{HV}/I_{HH}.

The morphology of the polymer aggregates was examined using atomic force microscope (AFM; DI NanoScope IIIa). After P-3,*m* had formed aggregates in the mixed solvents, a drop of the solution with a concentration of about 1×10^{-4} g/mL was placed on the carbon-coated mica surface at room temperature, with the excess solution blotted by a filter paper. The sample was dried under ambient conditions and later in vacuum. The AFM height and phase images of the samples were recorded using taping mode, wherein the cantilever force was controlled to be large enough to explore the surface feature yet small enough to avoid sample damage.

The aggregate structures were further examined by wide-angle X-ray diffraction (WAXD) using a Bruker D8Discover diffractometer with a 3 kW ceramic tube as the X-ray source (Cu Kα) and a GADDS detector. To obtain enough amounts of the WAXD samples, stock solutions with relatively high concentrations ($\sim 10^{-2}$ g/mL) were used. After the aggregates were formed in the solvent mixtures, the solutions were left to dry slowly in test tubes at room temperature until the solvents were completely evaporated. The deposits were carefully collected from the test tube bottoms and then mounted on the sample stage of the Bruker D8Discover in a transmission mode. The diffraction peak positions were calibrated with silicon powder ($2\theta > 15°$) and silver behenate ($2\theta < 10°$). Background scattering was recorded and subtracted from the sample patterns. For comparison, WAXD patterns of the P-3,*m* bulk samples cooled from their isotropic state to room temperature were measured.

Results and Discussion

The P-3,*m* samples can be easily dissolved in common organic solvents (chloroform, THF, benzene, toluene, etc.). Since the polyacetylene backbone is typically insoluble, the good solubility of P-3,*m*s must be attributed to their side chains. When using a solvent common for the whole side chains, the P-3,*m* solutions are bright yellow and transparent. In this case, it is hard to discern the different affinities of the mesogenic core and alkyl tail. Our research is concerned with how the polymers will response when the solvent is tuned to be selective for the alkyl tails. For this purpose, we gradually added, for example, *n*-dodecane, into the chloroform solutions of P-3,*m* with the initial concentration higher than 1×10^{-5} g/mL. It was intriguing that the P-3,*m* solutions rendered a yellowish hue after a sufficient amount of *n*-dodecane was added, implying that a sort of aggregate was formed. When other alkane or cycloalkane as the selective solvent for the alkyl tails was used, similar phenomenon was observed.

The solutions of P-3,*m* with yellowish hue were stable for months, highly reminiscent of the solution self-assembly of surfactants or block copolymers. To determine the conditions of possible solution assembly or aggregation, we measured the change in the solution turbidity of P-3,*m* with the addition of selective solvent. Figure 1a shows the rapid increase in turbidity when the volume ratio of the selective solvent to chloroform exceeds a critical value. The onset of the turbidity increase depends on the tail length and the solvent property. That is, decreasing *m* or using a selective solvent with a larger carbon number leads to the earlier onset of the turbidity increase. The turbidity of P-3,*m* also exhibits a temperature dependence. For

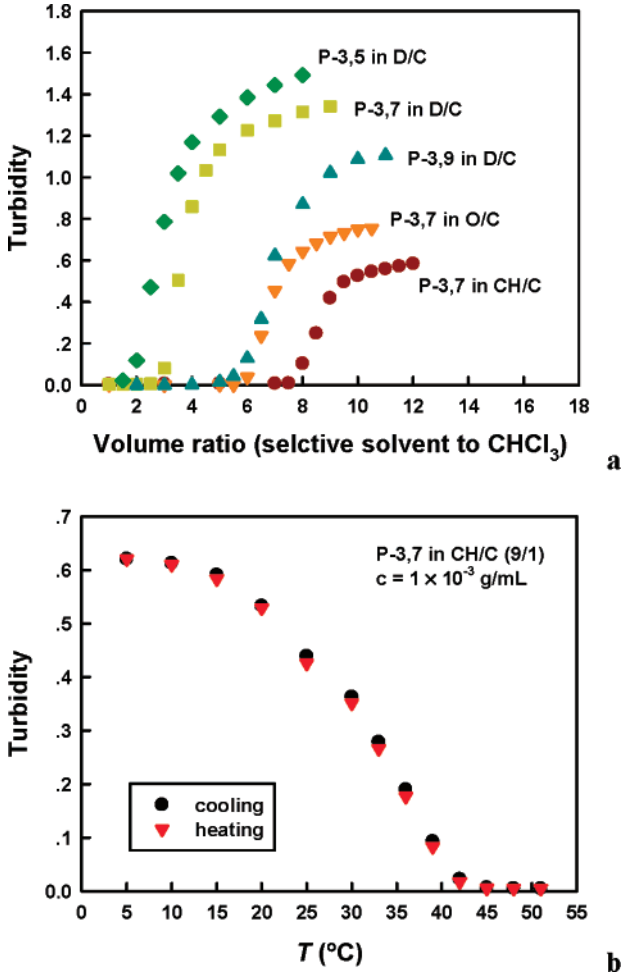

Figure 1. (a) Solution turbidity of P-3,*m* as a function of volume ratio of selective solvent to chloroform. C, chloroform; D, *n*-dodecane; O, *n*-octane; CH, cyclohexane. The initial concentration was 1×10^{-3} g/mL. (b) Temperature dependence of the turbidity of P-3,7 solution (1×10^{-3} g/mL) in CH/C (v/v = 9/1). The cooling is followed by the subsequent heating.

example, with a fixed CH/C volume ratio of 9/1, Figure 1b shows the change in turbidity of the P-3,7 solution (1×10^{-3} g/mL) with temperature. The solution hue disappears at high temperature. Upon cooling to below 45 °C, the yellowish hue reappears, and the turbidity continuously increases to reach a plateau after 20 °C. During the subsequent heating, the turbidity decreases, the value of which is almost identical to that measured during cooling at each temperature.

The procedures of selective solvent titration and of lowering temperature of the solvent mixture with fixed solvent composition shall progressively decrease the solvating power of the medium. Therefore, the aggregation or assembly of P-3,*m*s shall be ascribed to be solvent quality induced. The thermal behavior depicted in Figure 1b is of particular interest. For the reversible processes, the turbidity change upon cooling is superposed with that upon heating, indicating that almost no undercooling is required to form the polymer aggregates. The transition is thus close to thermodynamic equilibrium, similar to that occurred in liquid crystalline systems. The temperature range of transition looks broad (also see below, Figures 7 and 10). We speculate that the continuous worsening of the solvent quality with lowering temperature shifts the equilibrium to forming more aggregates. Moreover, for the sample with a rather broad MW distribution, its low MW components, which are more soluble in the solvent mixture, will finally incorporate into the aggregates when the turbidity reaches plateau at sufficient low temperatures.

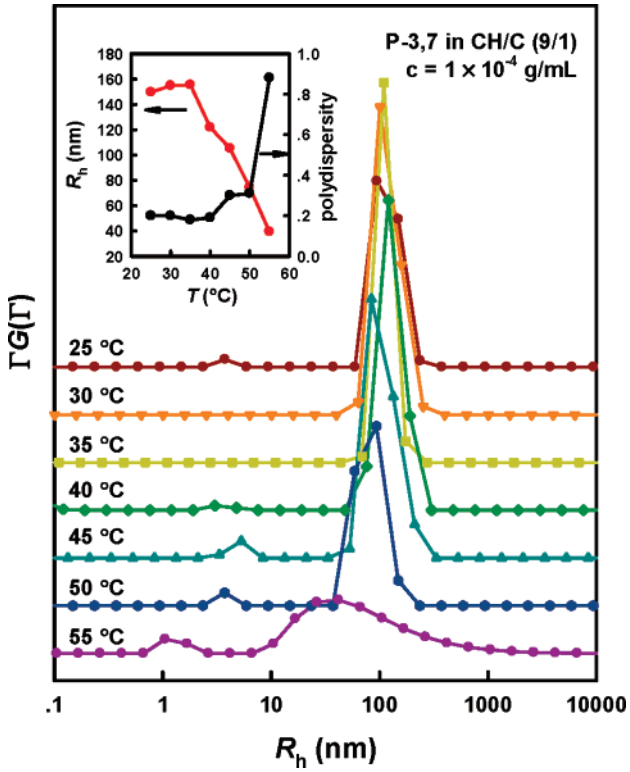

Figure 2. Set of hydrodynamic radius distributions of P-3,7 solution (1×10^{-4} g/mL) in CH/C (v/v = 9/1) at different temperatures measured upon cooling. The inset shows the temperature dependences of the peak position and the polydispersity of the aggregates.

As the turbidity measurements cannot elucidate the size evolution of the aggregates, we used DLS to monitor in situ the assembly process of P-3,7 in CH/C (v/v = 9/1) upon cooling, although the DLS measurements might only give the apparent size of the aggregates. Figure 2 illustrates the distributions of the apparent hydrodynamic radius (R_h) for the P-3,7 solution (1×10^{-4} g/mL) measured at an angle of 30° at various temperatures. Similar DLS data were obtained at other angles. In Figure 2, while the peak at $R_h < 10$ nm shall correspond to the unimers, dimers, and/or trimers, the peak at $R_h > 10$ nm can be attributed to the aggregates or clusters of the P-3,7 molecules. At 55 °C, the distribution peaked at 40 nm is rather board, the polydispersity of which is 0.9. It is worth noting that when the solution is cooled to 50 °C, the peak moves to 80 nm and its polydispersity abruptly drops to 0.3. With further lowering of temperature, the peak position continuously shifts to larger R_h and reaches a plateau of nearly 160 nm after 35 °C, and meanwhile, the polydispersity decreases to around 0.2 (see the inset). We consider that the drastic change in the R_h distribution at 55−50 °C is associated with the occurrence of molecular aggregation. The rather board peak at 55 °C may be attributed to a sort of density fluctuation caused by the insoluble polyacetylene backbones that always tend to cluster together in solution. In this case, some domains with a higher concentration than the average may appear dynamically in solution. At 50 °C, the P-3,7 molecules start to form aggregates with more dense packing, giving the new R_h distribution as shown in Figure 2. Compared with the onset of the turbidity rise in Figure 1b, the transition temperature of 50 °C measured by DLS is higher. This may be due to that DLS is much more sensitive to the appearance of the large aggregates.

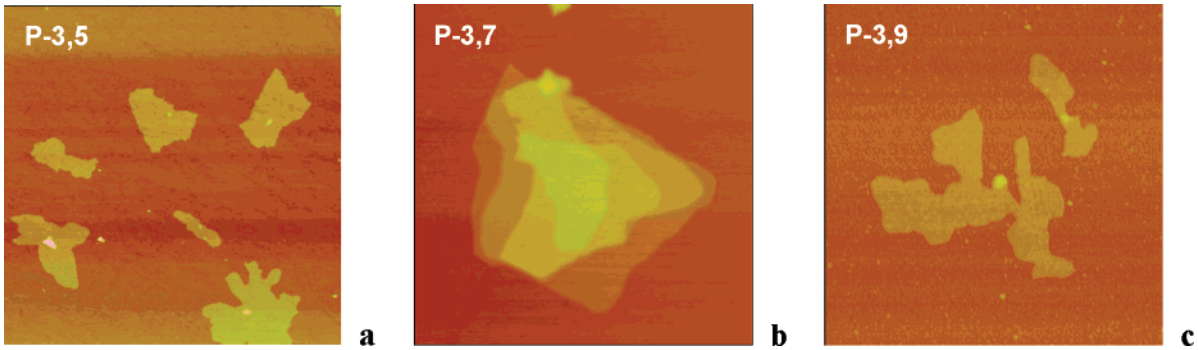

Figure 3. AFM height images of the P-3,*m* monolayer lamellae deposited on the carbon-coated mica surfaces: (a) P-3,5 (6 × 6 μm^2); (b) P-3,7 (2.5 × 2.5 μm^2); (c) P-3,9 (2.5 × 2.5 μm^2). In (b), overlapping of the monolayer lamellae can be seen.

To visualize the morphology of the P-3,*m* aggregates, we performed AFM experiments on the samples deposited on the carbon-coated mica surfaces after complete removal of the solvents at room temperature. Compared with the selective solvents, chloroform evaporated faster due to its higher vapor pressure. Therefore, the morphology of the aggregates in solvent mixtures could be "frozen" and remained in the final dry state. Figure 3 shows the AFM height images of P-3,*m*, which reveal that the aggregate morphology can be typically lamellar. On the substrates, the monolayer lamellae can deposit randomly (Figure 3, panels a and c) or partially overlap (Figure 3b). The lamellar shape is irregular and even dendritic, which may be because the molecules that packed together in the lamellae possess different chain lengths. On the other hand, the thicknesses of lamellae are rather uniform, which are measured to be around 3.8, 4.2, and 4.5 nm for the samples with $m = 5$, 7, and 9, respectively. Note that the calculated molecular widths (i.e., twice of the side-chain length) with an assumption of all-trans conformation of the methylene units are 4.3, 4.8, and 5.3 nm for $m = 5$, 7, and 9, respectively.[26] In comparison with these calculated dimensions, the measured thicknesses are slightly smaller. However, the correlation between them indicates that the lamellar thickness is largely determined by the molecular width.

The lamellar structure of the P-3,*m* aggregates can also be inferred from our WAXD experiments. To prepare the WAXD samples, we slowly dried the aggregate solutions in test tubes at room temperature. After the solvents were completely evaporated, the deposits carefully collected from the test tube bottoms were subjected to the WAXD experiments, the results of which are shown in Figure 4. For comparison, Figure 4 also includes the WAXD powder patterns of the bulk P-3,*m* samples which were cooled from their isotropic state to room temperature. As mentioned before, P-3,*m* in bulk state forms a highly ordered smectic phase with a frustrated molecular packing.[26] As shown by the dashed lines in Figure 4, the bulk P-3,*m* gives a second-order diffraction corresponding to a *d* spacing which is rather close to the calculated side-chain length. However, the scattering vector ratio of the first- and second-order diffractions is nearly 1.3, 1.3, and 1.5 for the bulk P-3,*m* with $m = 5$, 7, and 9, respectively, featuring the highly ordered smectic structure. For the dried deposits (see the solid lines), also two diffractions in the low 2θ angle region can be observed (for the second-order diffraction of the P-3,9 deposit sample, see the enlarged part of the curve). While the second-order diffraction locates at the position almost the same as that observed in the bulk sample, it is worth noting that the first-order diffraction of the deposit shifts greatly to lower angle, resulting in the scattering vector ratio of approximately 1:2. This evidences a smectic A structure with the layer period close to

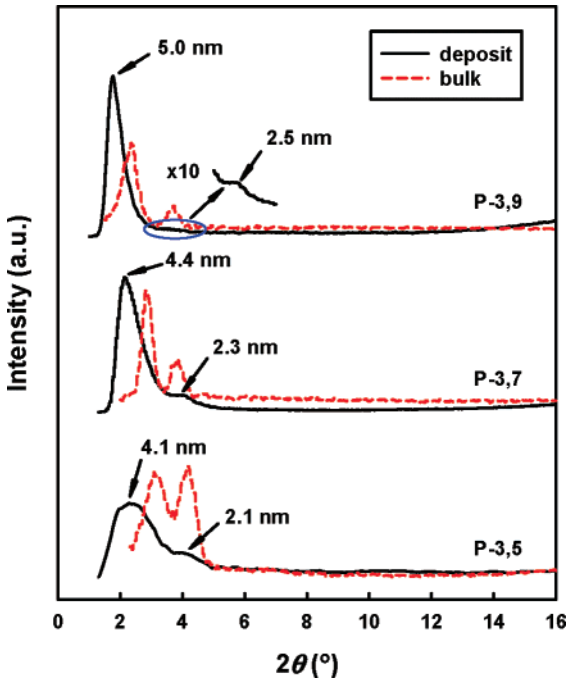

Figure 4. WAXD powder patterns of the bulk samples (dashed lines) and the solvent free deposits obtained by drying the aggregate solutions of P-3,*m*s (solid lines). For P-3,5 and P-3,7, the selected solvent used to induce the aggregation was cyclohexane; for P-3,9, the selective solvent was *n*-dodecane.

the molecular width of P-3,*m*. We consider that the deposits obtained by drying solutions are the stacking of lamellae. When the solvent is evaporated slowly, the gravitational forces will lead the floating monolayer lamellae in solution to gradually deposit layer by layer at the tube bottom. Eventually, the smectic A structure is formed in the solvent-free state.

On the basis of the experimental results of AFM and WAXD, we propose that the lamellae are formed by the sheetlike molecules of P-3,*m* with the backbones located in the lamellar center. As schematically depicted in Figure 5, within each molecular sheet, the side chains are parallel but extend to opposite directions on both sides of the backbone. Therefore, both top and bottom of the lamellae are the layers of alkyl tails, which can protect the solvophobic components of the polymers. Since the backbones and mesogenic cores on the side surfaces of the lamellae are still exposed to solvents, the lamellae can grow in lateral dimensions to reduce the free energy, resulting in the relatively large lamellae as shown in Figure 3. The alkyl tails may lose the all-trans conformation when packing into the monolayer lamellae, and/or the side chains may slightly incline with respect to the lamellar surface normal. Therefore, the monolayer thickness measured by AFM is slightly smaller

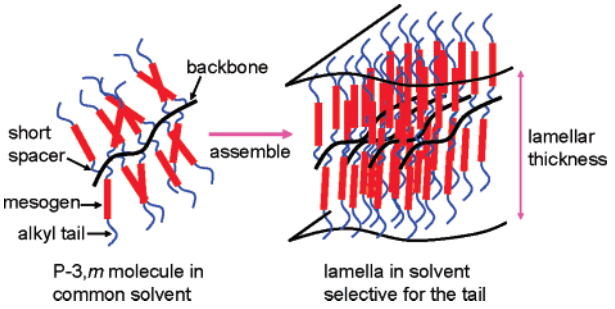

Figure 5. Schematic illustration of the lamellar structure formed by P-3,*m* in selective solvent. Within the lamella, the P-3,*m* molecules are sheetlike and pack parallel with each other, and the backbones are in the lamellar center. The lamellar thickness is determined by the width of the sheetlike molecule.

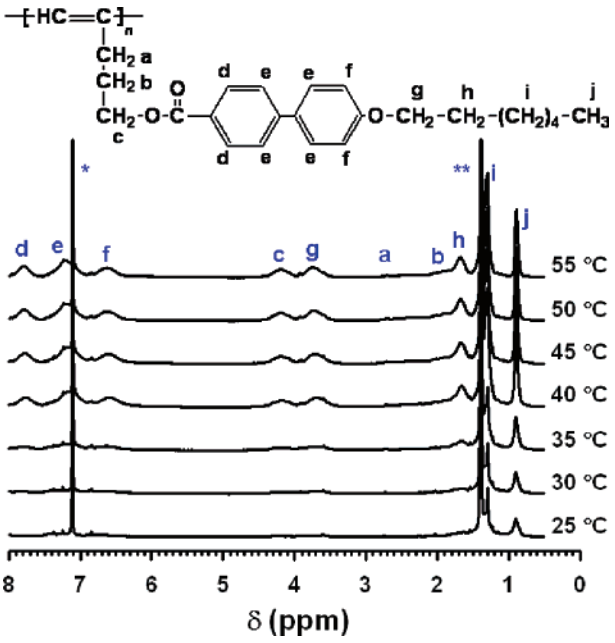

Figure 6. Set of ^{1}H NMR spectra of P-3,7 in CH/C (v/v = 9/1) (2×10^{-3} g/mL) recorded at different temperatures. The assignments of peaks a−j are shown. The peaks of the residual nondeuterated chloroform and cyclohexane are marked with * and **, respectively.

compared with the calculated molecular width of P-3,*m*. On the other hand, when the monolayer lamellae stacked together in the solvent-free deposits, solidification might make the tails be more extended, resulting in increased lamellar thickness (i.e., layer period determined by WAXD).

This packing model is supported by our solution ^{1}H NMR experiments. Figure 6 shows the ^{1}H NMR spectra of P-3,7 in CH/C (v/v = 9/1) with a concentration of 2×10^{-3} g/mL recorded at various temperatures, wherein the assignments of resonance peaks are included. When the P-3,7 molecules are sufficiently solvated at high temperatures, all the protons on the side chains are observable. Compared with that at 55 °C, the peak intensity becomes lower at 50 °C and decreases significantly at below 40 °C. In spite of the intensity reduction, the bands of the protons on the last four methylene and methyl groups of the tail (peaks i and j) can always be clearly identified at δ of 1.30 and 0.90 ppm, respectively. On the other hand, the peaks corresponding to the resonance of the protons in the inner part of the side chain, including those of the spacer (peaks a, b, and c), the biphenyl (peaks d, e, and f), and the first two methylene units in the alkyl tail (peaks g and h), decrease more abruptly in intensity with decreasing temperature. Consequently,

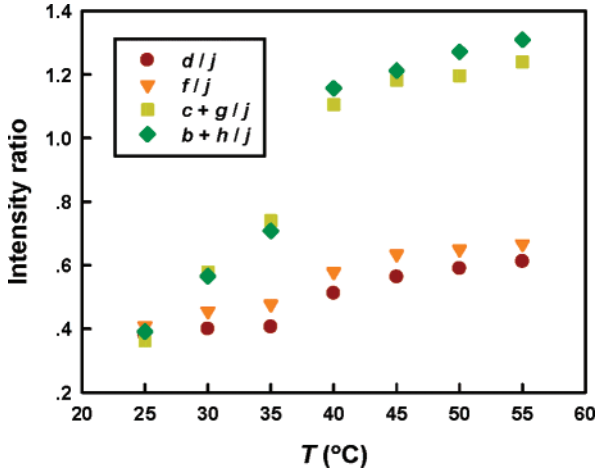

Figure 7. Change in the ratio of the integrated area of NMR peak d, f, c + g, or b + h to that of peak j as a function of temperature. For those peaks that are hard to be deconvoluted (e.g., peaks c and g at low temperatures in Figure 6), their combined areas are used.

their resonance signals become so weak and broad that they are hardly recognized in the spectrum measured at 25 °C.

Figure 7 presents the temperature dependence of the ratios of the integrated areas of NMR peaks d, f, c + g, and b + h to that of resonance peak j of the methyl protons. It is worth noting that at 55 °C the intensity ratios agree fairly well with the theoretical values. For example, the (b + h)/j is measured to be 1.31, which is close to the proton number ratio of 4/3. However, the ratios are decreased significantly with lowering temperature, the tendency of which is coincident with that observed in turbidity and DLS experiments, inferring again the assembly process. Moreover, the ^{1}H NMR spectral results reveal that the motions of the inner part of the side chain are highly restricted after assembly.[28] On the contrary, the parts of the alkyl tails far from the biphenyl remain mobile to a certain extent. This shall be attributed to their immediate interaction with the solvent molecules at or near the lamellar top and bottom surfaces where the environments are less rigid.

The P-3,*m* polymers are fluorescent due to the aromatic biphenyl groups that give the emission maximum at $\lambda_{em} = 360-380$ nm.[29] Figure 8 illustrates the UV−vis absorption and steady-state fluorescence spectra of P-3,7 in chloroform and CH/C (v/v = 9/1) at 25 °C. The molar concentrations of the polymer solutions were calculated on the basis of the repeating units of P-3,7. The UV−vis spectra of the polymer in chloroform and the CH/C mixture are almost the same (Figure 8a). Panels b and c of Figure 8 show the excitation and emission fluorescence spectra, respectively. In the excitation spectra, the fluorescence intensities of both the solutions are peaked at 310 nm. However, the emission maximum of the CH/C solution blue-shifts to 366 nm, compared with that at 373 nm for the chloroform solution in the emission spectra. Despite the same concentration, the fluorescence intensities of P-3,7 in CH/C (v/v = 9/1) are much lower than that in chloroform, due to the quenching of the light emission by the aggregate formation.

We carried out fluorescence anisotropy measurement to elucidate the molecular assembly process. Figure 9 shows the steady-state excitation anisotropy spectra at $\lambda_{em} = 370$ nm of P-3,7 in chloroform and the CH/C mixture (v/v = 9/1) with concentrations of 0.1 mM (or 4×10^{-5} g/mL) and 0.02 mM (or 8×10^{-6} g/mL). The chloroform solutions of P-3,7 display very low excitation fluorescence anisotropy, partially because of the relatively fast rotational diffusion of the molecules with $R_h < 10$ nm.[30] In addition, a strong resonance energy transfer

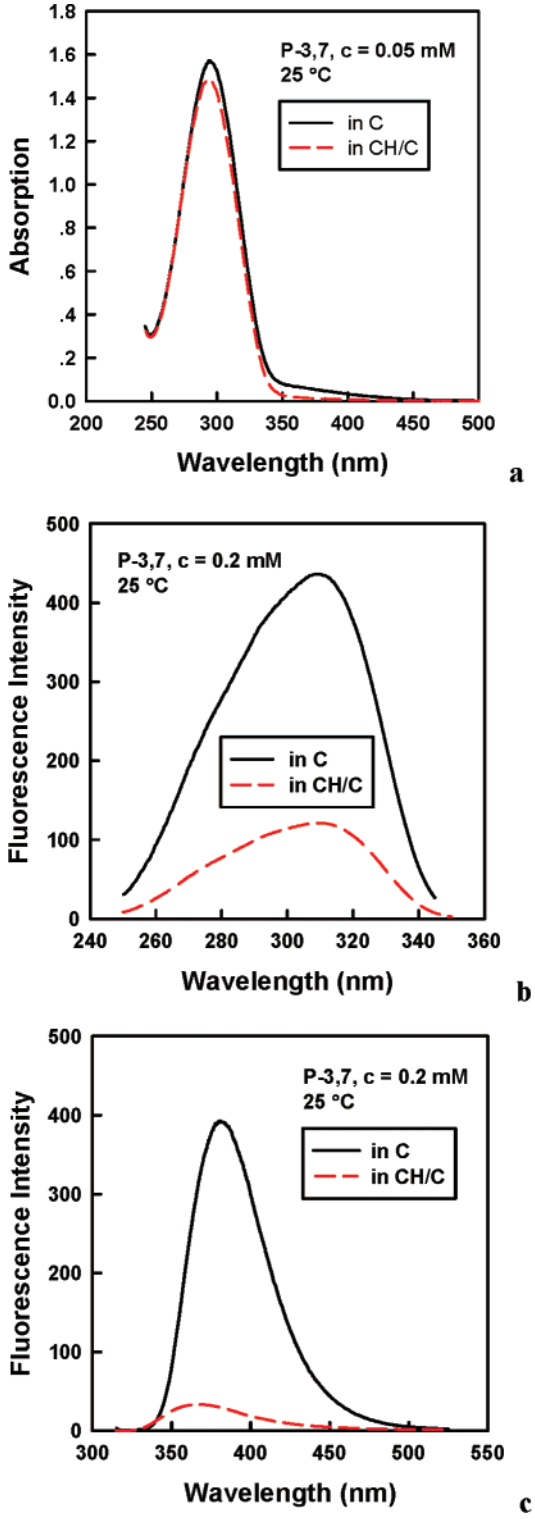

Figure 8. UV−vis absorption (a), steady-state excitation (b), and emission (c) fluorescence spectra of P-3,7 in chloroform (C) and CH/C (v/v = 9/1) at 25 °C.

induced by the high local concentration of the biphenyl can also reduce the anisotropy. However, although its fluorescence intensity is lower (see Figure 8b), P-3,7 in CH/C (v/v = 9/1) with a concentration of 0.1 mM at 25 °C exhibits a much higher fluorescence anisotropy in comparison with the chloroform solution. This shall be mainly due to that P-3,7 forms lamellae which possess a longer rotational correlation time.

Figure 10 presents the fluorescence anisotropy value r of P-3,7 at λ_{ex} = 320 nm and λ_{em} = 370 nm as a function of

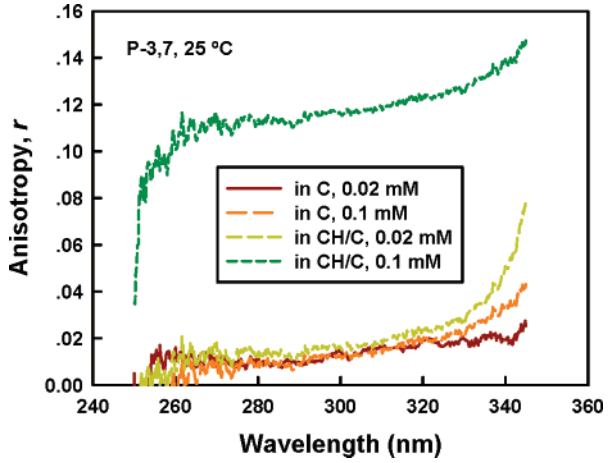

Figure 9. Excitation fluorescence anisotropy spectra at λ_{em} = 370 nm of P-3,7 in chloroform (C) and CH/C (v/v = 9/1) with two different concentrations (0.1 and 0.02 mM) at 25 °C.

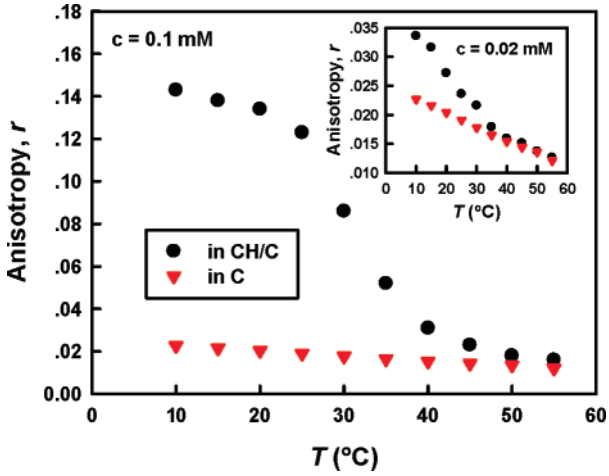

Figure 10. Excitation fluorescence anisotropy (r) change with temperature of P-3,7 in chloroform (C) and CH/C (v/v = 9/1) with concentrations of 0.1 and 0.02 mM (inset).

temperature. In Figure 10, the r value in chloroform increases almost linearly with decreasing temperature, which might be attributed to the rotational diffusion slowdown with the increase in solution viscosity. For P-3,7 in CH/C (v/v = 9/1) solution with the concentration of 0.1 mM, the r value is very close to that in chloroform when above 50 °C, wherein the polymer is well dissolved. Upon cooling to below 50 °C, the r value of the sample in CH/C increases significantly, indicating again the occurrence of P-3,7 assembly that will prolong the rotational correlation time. At below 25 °C, the r value is nearly 1 order of magnitude higher than that in chloroform.

In Figure 10, we also include the excitation fluorescence anisotropy data of a more dilute P-3,7 solution with a concentration of 0.02 mM (see the inset). For the CH/C solution with such a low concentration, DLS did not detect the large aggregates similar to that shown in Figure 2. Therefore, the concentration of 0.02 mM shall be lower than the cmc. Above 35 °C, the very dilute CH/C solution shares the same r value at each temperature with that in chloroform. However, the CH/C solution gives r values larger than those of the chloroform solution below 35 °C, and the difference gradually grows when the temperature decreases. We suspect that this phenomenon can arise from the rigidification of the P-3,7 molecules. As they are vertically linked to the backbone through a spacer of three methylene units and an ester group, the biphenyl groups get the freedom to align in various directions in common solvents.

The molecules are thus not sheetlike even if the backbone is assumed to be somewhat extended with a trans−cisoid conformation (see the left part of Figure 5). This orientation distribution of biphenyl may also contribute to the rather small *r*. When the solvating power of the mixed solvent becomes poorer at lower temperature, the biphenyl units might be forced to pack parallel with each other so that their contact with the poor solvent environment is minimized. In this case, the molecules are sort of stiffened to form the molecular sheet, resulting in larger *r* in the very dilute CH/C solution in comparison with that in the chloroform solution. We consider that such a possible molecular rigidification of P-3,7 may be tightly related to the lamellar formation. At a concentration above cmc, the two processes, namely, the molecular shape adjusting to be more sheetlike and packing together to form lamellae, may occur in sequence or simultaneously. However, to more clearly understand the lamellar formation requires more experiments. The research is currently ongoing in our laboratories.

Summary

In summary, we have investigated the self-assembly behaviors of the side-chain LC polyacetylene P-3,*m* in dilute solutions. The assembly processes were characterized by turbidity, DLS, ^{1}H NMR, and excitation fluorescence anisotropy of the polymer solutions. The morphology and structure of the resultant aggregates were examined using AFM and WAXD. The experimental results indicate that the P-3,*m* polymers form monolayer lamellae in solution when the solvent property is tuned to be selective for the alkyl tails of the side chains. In the lamella, the P-3,*m* molecules are sheetlike and pack parallel to each other with their backbones located at the lamellar center and the alkyl tails of their side chains on the top and bottom layers of the lamella. The lamellar thickness is largely determined by the width of the molecular sheet. When the solvent becomes selective for the tails, P-3,*m* may undergo shape stiffening to become sheetlike. We believe that similar assembly processes can be realized in other side-chain LC polymers. Moreover, the solution self-assembly of side-chain LC polymers with tremendous chemical varieties can provide rich phenomena with scientific value and technological implications.

Acknowledgment. This work was supported by National Natural Science Foundation of China (20129001, 20025414, and 50573001) and the Research Grants Council of Hong Kong (CA05/06.SC02). We are grateful to Prof. C. C. Han at the Institute of Chemistry of the Chinese Academy of Sciences for his useful discussion.

Supporting Information Available: Two-dimensional wide-angle X-ray diffraction patterns of highly ordered frustrated smectic structures of P-3,*m* ($m = 5, 7, 9$). This material is available free of charge via the Internet at http://pubs.acs.org.

References and Notes

(1) Ringsdorf, H.; Schlard, B.; Venzmer, J. *Angew. Chem., Int. Ed.* **1988**, *27*, 113−158.
(2) Percec, V.; Pugh, C. In *Side Chain Liquid Crystalline Polymers*; McArdle, C. B., Ed.; Chapman and Hall: New York, 1989; Chapter 3, pp 30−105.
(3) Ballauff, M. *Angew. Chem., Int. Ed.* **1989**, *28*, 253−267.
(4) Lam, J. W. Y.; Tang, B. Z. *Acc. Chem. Res.* **2005**, *38*, 745−754.
(5) Davidson, P. *Prog. Polym. Sci.* **1996**, *21*, 893−950.
(6) Godovsky, Y. K.; Makarova, N. N. *Philos. Trans. R. Soc. London A* **1994**, *348*, 45−57.
(7) (a) Percec, V.; Tomazos, D.; Heck, J.; Blackwell, H.; Ungar, G. *J. Chem. Soc., Perkin Trans. 2* **1994**, 31−44. (b) Percec, V.; Ahn, C.-H.; Cho, W.-D.; Jamieson, A. M.; Kim, J.; Leman, T.; Schmidt, M.; Gerle, M.; Möller, M.; Prokhorova, S. A.; Sheiko, S. S.; Cheng, S. Z. D.; Zhang, A.; Ungar, G.; D. J. P. *J. Am. Chem. Soc.* **1998**, *120*, 8619−8631. (c) Percec, V.; Ahn, C.-H.; Ungar, G.; Yeardley, D. J. P.; Möller, M.; Sheiko, S. S. *Nature (London)* **1998**, *391*, 161−164.
(8) (a) Schlüter, A. D. *Top. Curr. Chem.* **1998**, *197*, 165−191. (b) Schlüter, A. D.; Rabe, J. P. *Angew. Chem. Int. Ed.* **2000**, *39*, 864−883.
(9) (a) Tu, H. L.; Wan, X. H.; Liu, Y. X.; Chen, X. F.; Zhang, D.; Zhou, Q. F.; She, Z. H.; Ge, J. J.; Jin, S.; Cheng, S. Z. D. *Macromolecules* **2000**, *33*, 6315−6320. (b) Yin, X. Y.; Ye, C.; Ma, X.; Chen, E. Q.; Qi, X. Y.; Duan, X. F.; Wan, X. H.; Cheng, S. Z. D.; Zhou, Q. F. *J. Am. Chem. Soc.* **2003**, *125*, 6854−6855.
(10) (a) Finkelmann, H.; Lühmann, B.; Rehage, G. *Colloid Polym. Sci.* **1982**, *260*, 5665. (b) Lühmann, B.; Finkelmann, H.; Rehage, G. *Makromol. Chem.* **1985**, *186*, 1059−1073. (c) Jahns, E.; Finkelmann, H. *Colloid Polym. Sci.* **1987**, *265*, 304−311. (d) Amigó-Melchior, A.; Finkelmann, H. *Colloid Polym. Sci.* **2002**, *280*, 207−217.
(11) Wintermantel, M.; Fischer, K.; Gerle, M.; Ries, R.; Schmidt, M.; Kajiwara, K.; Urakawa, H.; Watatoka, I. *Angew. Chem., Int. Ed.* **1995**, *34*, 1472−1474.
(12) Burgemeister, D.; Farrell, T.; Schmidt, C. *Macromol. Chem. Phys.* **2006**, *207*, 396−403.
(13) (a) Ikkala, O.; Brinke, G. T.; Buokolainen, J. *Macromolecules* **1995**, *28*, 7088−7094. (b) Wang, X. *J. Polym. Sci., Part B: Polym. Phys.* **1999**, *37*, 667−677.
(14) Laschewsky, A. *Adv. Polym. Sci.* **1995**, *124*, 1−86 and references therein.
(15) Cochin, D.; Candau, F.; Zana, R.; Talmon, Y. *Macromolecules* **1992**, *25*, 4220−4223.
(16) (a) Borisov, O. V.; Halperin, A. *Langmuir* **1995**, *11*, 2911−2919. (b) Rouault, Y. *Macromol. Theory Simul.* **1998**, *7*, 359−365. (c) Diamant, H.; Andelman, D. *Europhys. Lett.* **1999**, *48*, 170−176. (d) Subbotin, A.; Saariaho, M.; Ikkala, O.; Brinke, G. T. *Macromolecules* **2000**, *33*, 3447−3452.
(17) Kawaguchi, S.; Akaike, K.; Zhang, Z.-M.; Matsumoto, H.; Ito, K. *Polym. J.* **1998**, *30*, 1004−1007.
(18) (a) Wegner, G. *Macromol. Chem. Phys.* **2003**, *204*, 347−357. (b) Liu, T.; Rulkens, R.; Wegner, G.; Chu, B. *Macromolecules* **1998**, *31*, 6119−6128. (c) Rulkens, R.; Wegner, G.; Thurn-Albrecht, T. *Langmuir* **1999**, *15*, 4022−4025. (c) Backstaller, M.; Köhler, W.; Wegner, G.; Fytas, G. *Macromolecules* **2001**, *34*, 6353−6358.
(19) Schafheutle, M. A.; Finkelmann, H. *Liq. Cryst.* **1988**, *3*, 1369−1386.
(20) (a) Halperin, A.; Tirrell, M.; Lodge, T. P. *Adv. Polym. Sci.* **1992**, *100*, 31−71. (b) Tuzar, Z.; Kratochvil, P. In *Surface and Colloid Science*; Matijević, Ed.; Plenum: New York, 1993; Vol. 15; Chapter 1, pp 1−83. (c) Chu, B. *Langmuir* **1995**, *11*, 414−421. (d) Cameron, N. S.; Corbierre, M. K.; Eisenberg, A. *Can. J. Chem.* **1999**, *77*, 1311−1326. (e) Jain, S.; Bates, F. S. *Science* **2003**, *300*, 460−464. (f) Antonietti, M.; Förster, S. *Adv. Mater.* **2003**, *15*, 1323−1333.
(21) Ober, C. K. *Science* **2000**, *288*, 448−449.
(22) Sheiko, S. S.; Möller, M. *Chem. Rev.* **2001**, *101*, 4099−4123.
(23) (a) Yoshida, M.; Fresco, Z. M.; Ohnishi, S.; Fréchet, J. M. J. *Macromolecules* **2005**, *38*, 334−344. (b) Das, J.; Yoshida, M.; Fresco, Z. M.; Choi, T.-L.; Fréchet, J. M. J.; Chakraborty, A. K. *J. Phys. Chem. B* **2005**, *109*, 535−541.
(24) (a) Shinohara, K.-I.; Yasuda, S.; Kato, Y.; Fujita, M.; Shigekawa, H. *J. Am. Chem. Soc.* **2001**, *123*, 3619−3620. (b) Li, B. S.; Cheuk, K. K. L.; Ling, L.; Chen, J.; Xiao, X.; Bai, C.; Tang, B. Z. *Macromolecules* **2003**, *36*, 77−85. (c) Sakurai, S.-I.; Kuroyanagi, K.; Morino, K.; Kunitake, M.; Yashima, E. *Macromolecules* **2003**, *36*, 9670−9674. (d) Sakurai, S.-I.; Okoshi, K.; Kumaki, J.; Yashima, E. *Angew. Chem., Int. Ed.* **2006**, *45*, 1245−1248. (e) Sakurai, S.-I.; Okoshi, K.; Kumaki, J.; Yashima, E. *J. Am. Chem. Soc.* **2006**, *128*, 5650−5651.
(25) (a) Percec, V.; Rudick, J. G.; Peterca, M.; Wagner, M.; Obata, M.; Mitchell, C. M.; Cho, W. D.; Balagurusamy, V. S. K.; Heiney, P. A. *J. Am. Chem. Soc.* **2005**, *127*, 15257−15264. (b) Percec, V.; Aqad, E.; Peterca, M.; Rudick, J. G.; Lemon, L.; Ronda, J. C.; De, B. B.; Heiney, P. A.; Meijer, E. W. *J. Am. Chem. Soc.* **2006**, *128*, 16365−16372.
(26) Ye, C.; Xu, G.-Q.; Yu, Z.-Q.; Lam, J. W. Y.; Jang, J. H.; Peng, H.-L.; Tu, Y.-F.; Liu, Z.-F.; Jeong, K.-U.; Cheng, S. Z. D.; Chen, E.-Q.; Tang, B. Z. *J. Am. Chem. Soc.* **2005**, *127*, 7668−7669.
(27) Lam, J. W. Y.; Kong, X.; Dong, Y.; Cheuk, K. K. L.; Xu, K.; Tang, B. Z. *Macromolecules* **2000**, *33*, 5027−5040.
(28) (a) Spěváček, J. *Makromol. Chem., Rapid Commun.* **1982**, *3*, 697−703. (b) Candau, F.; Heatley, F.; Price, C.; Stubbersfield, R. B. *Eur. Polym. J.* **1984**, *20*, 685−690. (c) Wanka, G.; Hoffmann, H.; Ulbricht, W. *Macromolecules* **1994**, *27*, 4145−4159. (d) Low, A. B.; Billingham, N. C.; Armes, S. P. *Macromolecules* **1998**, *31*, 5991−5998.
(29) Huang, Y. M.; Ge, W.; Lam, J. W. Y.; Tang, B. Z. *Appl. Phys. Lett.* **1999**, *75*, 4094−4096.
(30) Lakowicz, J. R. *Principles of Fluorescence Spectroscopy*, 2nd ed.; Kluwer: New York, 1999; Chapter 10, pp 291−319.

MA0710028